
# GUST LOAD ALLEVIATION IN A SCALED UAV DEMONSTRATOR

Alexander Herwig[1,2], Matthias Haupt[1,2], Tristan Brack[1,2], Jorge Bustamante[1,2] & Sebastian Heimbs[1,2]

[1]Cluster of Excellence SE²A – Sustainable an Energy-Efficient Aviation, TU Braunschweig, 38108 Braunschweig
[2]Institute of Aircraft Design and Lightweight Structures (IFL), TU Braunschweig, 38108 Braunschweig

## Abstract

A mid-range aircraft design is scaled through a demonstrative scaling scheme to investigate the feasibility of implementing an active and passive gust load alleviation (GLA) for flexible wings to perform scaled flight tests. As highly significant parameters for the proposed gust load alleviation methods, the flexural stiffness and natural frequency of the scaled wing are characterized through static and dynamic experiments.

**Keywords:** gust load alleviation, UAV, aeroelasticity, scaled demonstator

## 1. Introduction

As a result of global warming and climate change, the aviation industry is undergoing significant changes to achieve sustainable civil aviation with a reduced ecological footprint. A major effort to define these climate goals is the Flightpath 2050 of the European Advisory Council for Aeronautics Research (ACRE) that sets emission reduction targets of 74 % for $CO_2$ and 90 % for $NO_x$ compared to a modern aircraft from 2000 [1]. To have any chance of meeting these very ambitious targets, disruptive breakthrough technologies are needed to achieve significant improvements in overall aircraft efficiency.

One way to increase the efficiency of an aircraft is to tailor it to a specific transportation task. The Cluster of Excellence SE$^2$A - Sustainable and Energy-Efficient Aviation - at the Technische Universität Braunschweig is pursuing this approach by developing specialized aircraft configurations for short-, medium-, and long-haul flights. The development is driven by the preliminary aircraft research group under the assumption of future technology availability and improvements. The assumed effectiveness and impact on the overall design is typically assessed by statistics or experience. Unfortunately, while both are urgently needed, neither is readily available for unconventional aircraft or novel technologies nor their interactions. Promising weight-saving technologies such as gust load alleviation (GLA) and maneuver load alleviation (MLA) methods, which reduce the wing root bending moment while also increasing passenger comfort are examples of the technological assumptions made in the proposed preliminary designs. Especially when both are combined since significant portions of the primary wing root structure of typical modern CS 25 aircraft are often sized by gust load cases [2].

Therefore, the researchers within SE$^2$A work in a multidisciplinary team to explore technologies and processes that have the potential to enable a sustainable and energy-efficient aviation, in order to find holistic solutions to improve the sector as a whole. One building block within SE$^2$A that aims to prove the technology assumptions made in the preliminary design is a scaled UAV. In this research, the scaled gust load alleviation technology demonstrator performing load alleviation experiments in scaled flight tests is presented.

The present research will focus on evaluating whether the proposed GLA can be demonstrated in a scaled flight experiment. Therefore, the parameters of the reference aircraft, the flight scale (FS), will be described, listed, and scaled to obtain the parameters of the model scale (MS). The derived scaling factors are discussed and adjusted to meet regulatory requirements. This is followed by an experimental investigation that evaluates the bending stiffness and natural frequencies of a stiffened 3D printed wing. The wing is designed according to the scaled parameters, demonstrating that the scaled parameters can be achieved by the chosen design and manufacturing process.

## 2. The Full Scale Reference

The SE$^2$A MR V4 BW shown in Fig. 1a is an intermediate result of the preliminary aircraft design junior research group within SE$^2$A. The aircraft is designed to be efficient in a harmonic range of $4.000\,\mathrm{km}$ and has a backward swept wing with a high aspect ratio to reduce lift-induced drag. The two engines are mounted above the wings. The cruise altitude is designed to be at $7.650\,\mathrm{m}$ with a cruise Mach number of $0.71$. The described cruise flight conditions are chosen as reference flight state used in the scaling scheme. The total weight of the aircraft is assumed to be $\mathrm{MTOW} = 61.225\,\mathrm{kg}$, directly after take-off. A detailed description of the configuration and reasoning in the design choices made by Karpuk et al. can be found in [3]. The parameters of the FS and MS used in the scaling can be found in Tab. 1. Since the configuration is the result of a preliminary design, the rough parameters describing the aircraft and its external shape are known, but no detailed internal geometry is available for scaling.

Table 1 – Summary of the SE2A MR V4 BW full scale and model scale parameters and the resulting scaling factors, grouped by set scaling, externally defined values, atmospheric data, and calculated based on the scaling scheme.

| parameter | variable | equation | unit | flight scale | model scale | scaling factor |
|---|---|---|---|---|---|---|
| Froude number | $Fr$ | $V^2/L\cdot g$ | 1 | 113.45 | 113.45 | 1.0000 |
| Relative density | $RD$ | $m/\rho\cdot L^3$ | 1 | 1.40 | 1.40 | 1.0000 |
| Flight altitude | $h$ | - | m | 7,650 | 100 | 0.0131 |
| Mass | $m$ | $\rho V$ | kg | 62,715 | 25 | 0.0004 |
| Atmospheric density | $\rho_{air}$ | | kg/m³ | 0.55 | 1.21 | 2.2179 |
| Kinematic viscosity | $\mu$ | ICAO [4] | m²/s | $2.84\cdot10^{-5}$ | $1.49\cdot10^{-5}$ | 0.5251 |
| Speed of sound | $c$ | | 1 | 309.54 | 339.91 | 1.0981 |
| Velocity | $V$ | $\sqrt{Fr\cdot L\cdot g}$ | m/s | 219.77 | 52.21 | 0.2376 |
| Mach number | $Ma$ | $V/c$ | - | 0.71 | 0.15 | 0.2163 |
| Reynolds number | $Re$ | $V\cdot L/\mu$ | - | $4.95\cdot10^7$ | $1.26\cdot10^6$ | 0.0255 |
| Dynamic pressure | $p_{dyn}$ | $\frac{1}{2}\rho\cdot V^2$ | kg/(ms)² | 13,211 | 1,653 | 0.1252 |
| Wingspan | $b$ | $m/(RD\cdot\rho\cdot m)^{1/3}$ | m | 43.3 | 2.45 | 0.0564 |

The proposed active gust load alleviation investigated in SE$^2$A uses an aeroelastic flight dynamic model. In order reduce the wing root bending moment, (fast) flaps placed along the trailing edge and actuated in order to reduce individual bending modes of the aircraft wing, exemplary shown in Fig. 1b. A description of the system is given by Bauknecht et al. [5] and Beyer et al. [6]. Passive gust load alleviation is achieved using a flared hinge concept comparable to the approach described by Cooper et al. [7] and Meyer et al. [8]. However, instead of an actual hinge, a non-linear deformation of the wing box combined with a local buckling of the inner wing structure is used to achieve the flared hinge, which reduces the gust loading of the structure [9, 10]. A numerically calculated example of the desired deformation is shown in Fig. 2. Due to the use of a bending torsion coupling that reduces the local lift by bending upward, the passive load alleviation methods cannot be realized in a forward-swept wing. Therefore, the SE$^2$A mid-range configuration *MR V4 BW* with backward swept wings, shown in Fig. 1, was chosen as the demonstrator used for scaling.

## 3. The Model Scale

Full aeroelastic scaling is desired to match the aeroelastic behavior. Unfortunately, this is generally not possible [11, 12]. Therefore, a demonstrative scaling approach has been chosen, where only the relevant parameters or sections of the aircraft are scaled by applying the appropriate scaling laws [13]. The scaling factor of the Froude number is set at $k_{Fr} = 1$, while the geometric scaling factor of

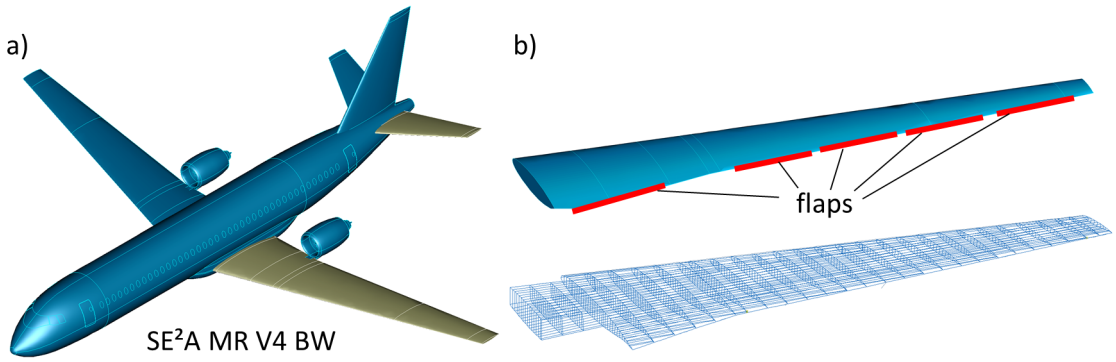


Figure 1 – a) Mid-range passenger aircraft developed in the SE$^2$A cluster the SE$^2$A MR V4 BW. b) Wing with flap distribution for active load distribution and model used in the finite element analysis.

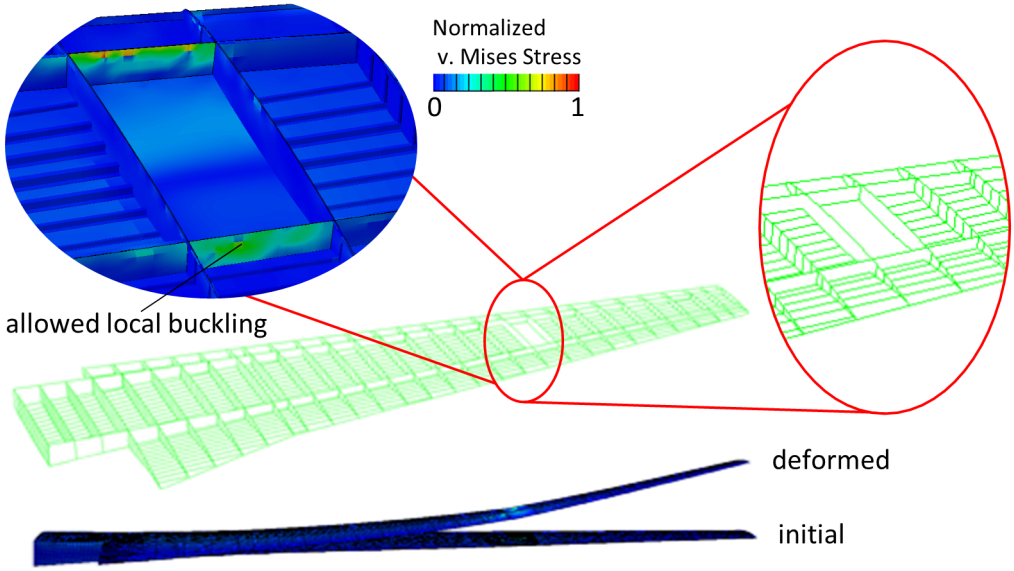


Figure 2 – Example of a wing with a structural flared hinge by allowing a non-linear deformation of the wing box [9].

$k_b = 0.056$ between the aircraft and the model scale is given by the wingspan of the MR V4 and the requirement to remain in the open flight category of EASA for civil drones, which limits the weight to less than $25\,\mathrm{kg}$. The flight range is limited to VLOS and an altitude of $120\,\mathrm{m}$. An appropriate similarity of the corresponding natural frequencies and normal modes between the model and flight scale is achieved by adjusting the mass and stiffness distributions according to the scaling laws while freely modifying the internal structure. Due to the required geometric scaling factor, the natural frequencies are expected to increase by a factor of $k_\omega \approx 4.2$. This requires fast actuators to be used in the active GLA and also increases the deformation speed necessary in passive load alleviation concepts. In the proposed GLA, the first bending mode of the wing is reduced. Therefore, the first natural frequency and the mass distribution of the wing are considered as the most important scaling characteristics.

## 3.1 Scaling Parameters

The parameters used in scaling can be derived from the fundamental equations. In case of an aircraft, these are the fundamental equations describing the physics of flight. The forces and moments experienced by an aircraft are generally a function of the aircraft and fluid properties, motion characteristics, and gravitational effects and can be described by seventeen properties, shown in Eq. 1, involving three fundamental units: length, time, mass [14, 15, 16].

$$F, M = f(\overbrace{\rho, \mu, c,}^{\text{fluid prop.}} \overbrace{l, \delta, m, I, EI', GJ',}^{\text{aircraft prop.}} \overbrace{\alpha', V, \alpha, \Omega, \dot{\Omega}, \omega,}^{\text{motion characteristics}} \overbrace{g, t}^{\text{gravity, time}}) \tag{1}$$

The physical properties can also be expressed as nondimensional parameters. The dimensional analysis of Buckingham [17] leads to Eq. 2, which states that 14 nondimensional parameters are needed to define similarity. The input properties of the resulting nondimensional parameters are shown in Eq. 3 [11].

$$\text{No. of non-dimensional parameters} = \text{No. of physical quantities} - \text{No. of fundamental units} \tag{2}$$

$$C_F, C_M = f\left(\frac{\rho V l}{\mu}, \frac{V}{c}, \delta, \frac{m}{\rho l^3}, \frac{I}{\rho l^5}, \frac{EI'}{\rho V^2 l^4}, \frac{GJ'}{\rho V^2 l^4}, \alpha', \frac{al}{V^2}, \frac{\Omega l}{V}, \frac{\dot{\Omega} l^2}{V^2}, \frac{\omega l}{V}, \frac{V^2}{lg}, \frac{tV}{l}\right) \tag{3}$$

During the design of a scaled model, the relevant aspects to be scaled have to be chosen depending on the planned investigation subject. Sobron et al.[11] give an extensive overview of the similarity parameters and scaling approaches of recent projects performing scaled flight tests (SFT). They further define four common scaling approaches used in SFT experiments: Aerodynamic scaling, dynamic scaling, aeroelastic scaling and demonstrative scaling. Depending on the archived scaling, they also define the required matching similarity parameters. Additionally, they also state that the proposed scaling groups should be seen as a guideline, since currently there is no general definition. This is especially true for the demonstrative scaling, where, at the discretion of the performing researcher, only the relevant properties are matched.

The first bending mode, which lifts both wings symmetrically, results in the highest wing root bending moment. For the flight scale SE$^2$A MR V4 BW this first bending mode is expected to occur at a frequency of $9.8\,\mathrm{Hz}$. The equivalent time scaling at $k_t \approx 0.24$ can be calculated directly from the Froude number and the geometric scaling, resulting in a frequency of $41\,\mathrm{Hz}$ for the MS. The required actuator speed and actuation frequency are assumed to be achievable with fast actuators and specialized flaps. However, the airflow and resulting lift depend on the Reynolds and Mach number and must also be able to react fast enough to provide an effective GLA. By requiring a similitude of the Froude Number, both, the Reynolds and Mach Number cannot be correctly scaled due to the nonlinear influence of the Velocity on the three parameters. Due to the low velocity of the MS, the Mach number mismatch should have little influence. Whether this is also holds true for the fast actuators remains to be investigated.

Generally the best scaling that can be achieved is also preferred by researchers, but due to the regulatory requirements the total mass of the aircraft is limited to less than 25 kg, also the altitude above ground (AGL) of $h \leq 120\,\mathrm{m}$ must not be exceeded. Therefore, the atmospheric properties air density, kinematic viscosity and speed of sound are also fixed. This, together with the chosen matching Froude number $Fr$ and relative density $RD = Fr = RD = 1$ leads to a reduction of variable parameters in Eq. 3 and the scaling factors shown in Tab. 1.

## 3.2 Wing Design and Flight Performance

In order to stay as close as possible to the original aircraft, the external shape should be changed as little as possible. Therefore, the general configuration, external shape, and planform were left untouched. This is especially true for the wing, its planform, stiffness and weight distribution, as these would directly affect the response to gust loads. The scaling scheme used results in a high wing loading. To generate the necessary lift, high landing and take-off speeds are required but must be limited to allow for manual control during the first flights. Therefore, the aerodynamics of several candidate airfoils for the scaled aircraft were compared in flight states such as takeoff, cruise, turn, and landing using the XFLR5 software. The airfoil of the FS was changed from the DRL15 profile to the SD7062 profile for the MS to improve the handling qualities and the lift force at low Reynolds numbers. This change better matches the flight conditions of the model scale and is expected to have little effect on the flexural behavior of the wing shown in Fig. 3.

The stiffener structure of the outer wing segment shown in Fig. 3a is made of carbon fiber reinforced plastic (CFRP) tubes with a diameter of $t = 10\,\mathrm{mm}$ and a thickness of $t = 2\,\mathrm{mm}$ and is designed to withstand 2.5g maneuvers. Bending tests were performed to assess the failure load of the tubes. Depending on the ply stacking, a bending stiffness of $E_{0,90} = 85.0 \pm 0.43\,\mathrm{GPa}$ and $E_{\pm 45} = 63.3 \pm 0.09\,\mathrm{GPa}$ was measured. The bending moment at failure of $M_{0,90,max} \approx 58.5\,\mathrm{Nm}$ is much higher than the loads induced into the wing structure by aerodynamic forces.

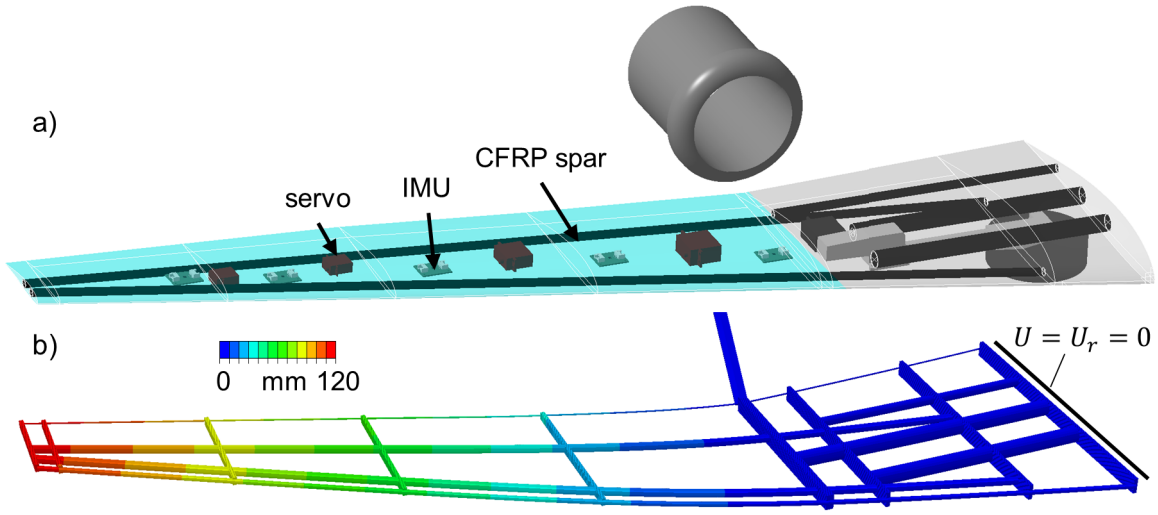


Figure 3 – a) Inner construction of the wing, positioning of the inertial measurement units (IMU) and servo actuators. b) Expected wing displacement at cruise flight (n=1) estimated by a beam elements in a finite element analysis.

## 4. Experimental Investigation

The experimental investigation evaluates the first iteration of the wing design as well as the production approach using a 3D printed outer shell that is stiffened by the CFRP structure with respect to the expected bending deformation and natural frequencies, since these are seen as the main parameters in the scaling of the proposed GLA methods. Another key aspect is the assessment of the influence of the printed structure on the bending deformation and dampening properties. In order to allow for a better interpretation of the measured data, the results obtained are compared to a commercially available radio-controlled plane (RC plane) the "Funray" with a comparable surface area and wing span of two meters from Multiplex [18]. The Funray aircraft is also used for preliminary electronics and flight tests demonstrating the active gust load alleviation. The Funray as a hole is much lighter than the MS, the wing weighs $290\,\mathrm{g}$. Together with the fuselage, motor, and additional electronics, the take-off weight is $2010\,\mathrm{g}$. The investigated wing section of the MS has a weight of $390\,\mathrm{g}$.
In order to avoid torsional vibrations of the engines, the inner wing section from the fuselage up to the engine is considerably stiffer, see Fig. 3b. Therefore, because of the research focus on elastic wing deformation, only the wing section beyond the engines is investigated. The investigation is performed in two steps. First, static bending under a concentrated force located at the tip of the wing and second, dynamic spring-back oscillation after an initial deflection. Both, the deformation as well as the oscillation are measured by digital image correlation (DIC) using the Zeiss Aramis with 12M-Pixel cameras for the static deformation and 1M-Pixel Photron Nova cameras for the frequency analysis.

### 4.1 Additive Manufacturing

There are several production technologies that can be used to build the outer structure of a scaled RC plane. In this project, fused deposition modeling (FDM) using light-weight polyactide (LW PLA) was chosen because of the capability to produce closed cavities and also the ability to easily perform geometry changes. The reduced density compared to conventional PLA is achieved by the addition of an active foaming agent that leads to a closed-pore PLA foam during the printing process. Depending on extrusion speed and printing speed, as well as temperature, the foaming percentage can be varied from 0 % to 60 % leading to densities between 0.53 and 0.62 g/cm³ and a stiffness in the range of $3,000$ to $1.050\,\mathrm{MPa}$. For the production of the wing structure, colorFabb's LW-PLA-HT material was used, as it is designed to be more resistant to prolonged exposure to heat [19]. In the performed printing process a line width of 0.4 mm a layer thickness of 0.2 mm, a temperature of 245 °C and a density of 0.73 g/cm³ were calibrated.

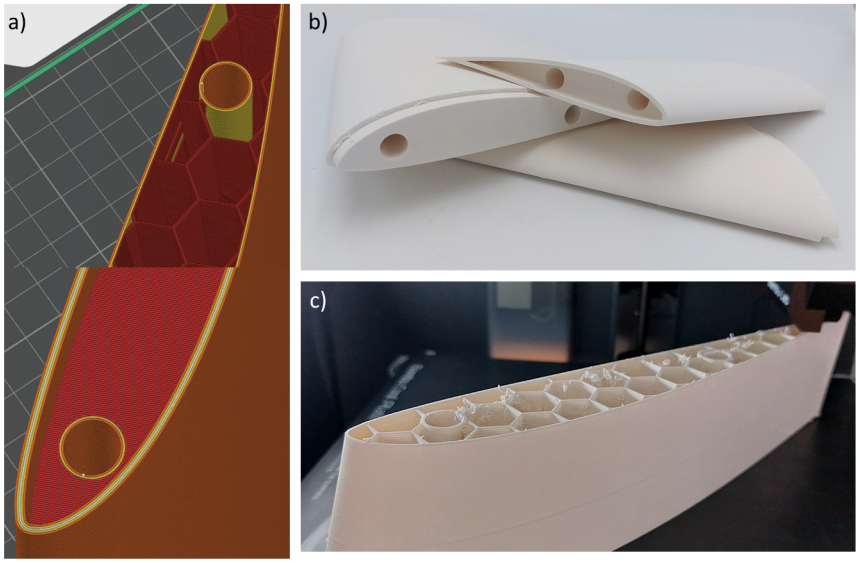


Figure 4 – a) Wing structure in as displayed in the slicer software showing the outer skin formed by four layers and the inner 5 %-honeycomb structure b) Joining interfaces between the individual wing segments c) LW-PLA structure during printing process.

## 4.2 Static Analysis

The simplified experimental setup is shown in Fig. 5. The clamping of the wing segment can be realized by either directly fixing the spars as well as the wing root structure and also a combination of both. In the conducted experiment, a 3D printed clamping was chosen to hold the CFRP spars in place, as this is believed to be comparable to the clamping mechanism found in the final demonstrator. An additional attachment of the wing root structure to the fuselage would stiffen the system and further increase the first natural frequency. A static load at the tip is used to induce a static deflection. Due to the wing orientation, the deflection orientation coincides with the bending due to the aerodynamic lift. The spatial deflection of the wing surface measured by the Zeiss Aramis 12M system using a 24 mm lens. Fig. 6a shows the experimental setup. An example measurement of the deflection in the z direction and the position of the evaluation line along the aerodynamic center is shown in Fig. 6b.

The deformation in the spanwise direction is evenly distributed and shows little torsion. This was expected due to the chosen load introduction point. The deformation along the evaluation line is shown in Fig. 7. When comparing the stiffening structure and the combination of the printed wing and the stiffening structure at a load of 9.81 N, it can be seen that the printed structure is responsible for approximately 23 % of the bending stiffness. Both can be well approximated by an equivalent beam. The biggest deviation from the expected deflection is located near the wing root. For a load of 18.5 N the deviation amounts to $0.3\,\mathrm{mm}$ and is proportional to the applied load. Along the evaluation line, the deflection of the Funray clearly shows segments of different stiffness and cannot be well approximated by a single beam, especially near the wing root. Also, when comparing the measured deflection, it is clearly visible that the stiffened printed wing has a higher flexural stiffness than the Funray wing. From the graphs shown in Fig. 7 the equivalent bending stiffness $EI_{equiv}$ can be approximated, see Tab. 2. The nearly identical equivalent stiffness values for both load levels suggest a linear deformation behavior with respect to the applied load.

Table 2 – Approximated bending stiffness of the investigated wing structures.

| | Wing @18.5 N | Wing @9.81 N | Stiffening structure | Funray wing |
|---|---|---|---|---|
| $EI_{equiv}$ | 54.39 Nm² | 53.67 Nm² | 44.33 Nm² | 33.40 Nm² |

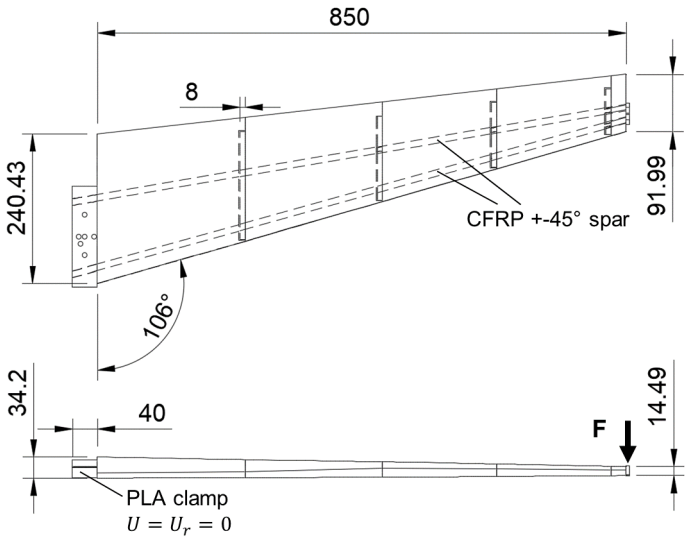


Figure 5 – Schematic representation of the experimental setup, specimen, and load application (dimensions in mm).

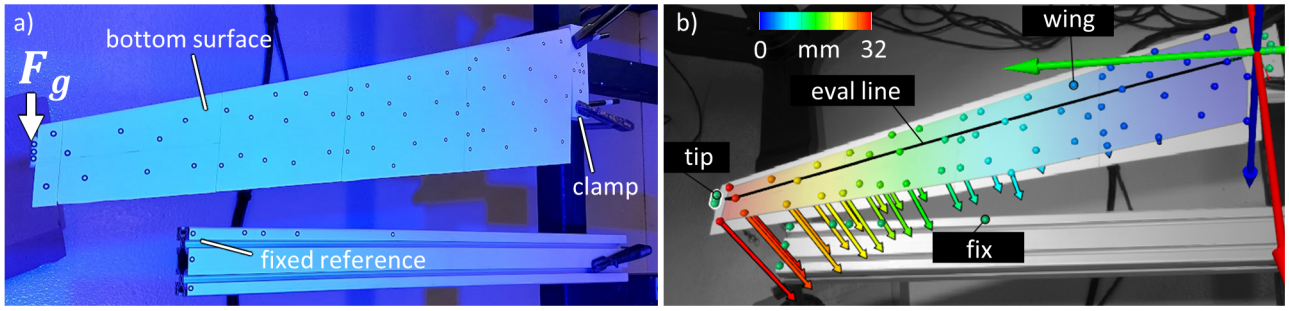


Figure 6 – a) Experimental setup used to measure the bending deformation of the wing structure. The bottom wing surface is mounted facing upwards. A weight at the wing tip is used to introduce the load bending the wing upwards in the aircraft coordinate system. b) Bending deflection on the bottom surface of the wing measured by DIC and position of evaluation line approximately along the aerodynamic center.

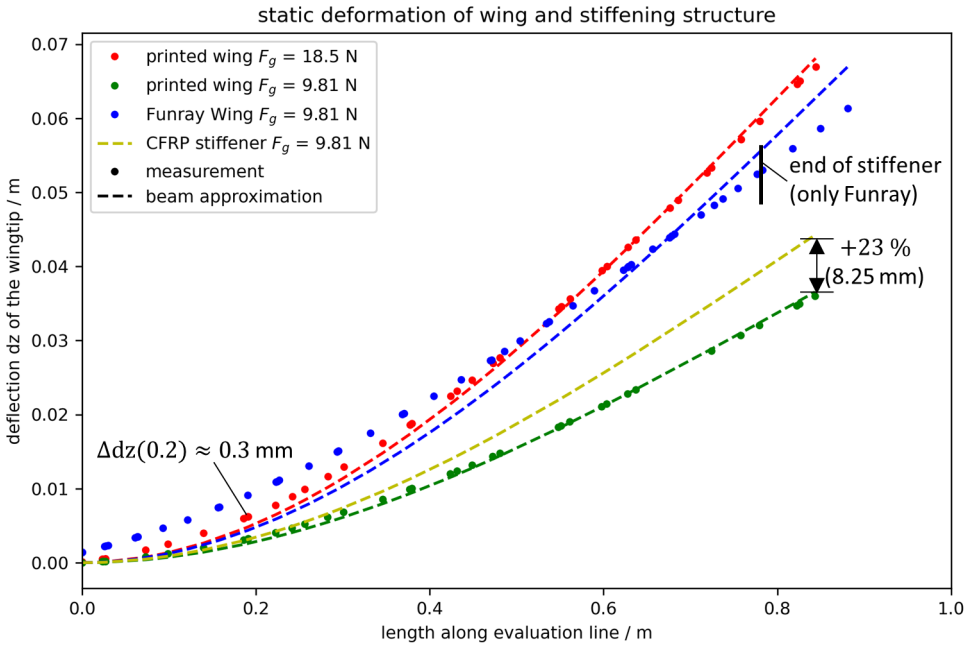


Figure 7 – Comparison of the static deformation of the stiffening structure, the stiffened printed wing and the commercial Funray Wing (stiffened Elapor).

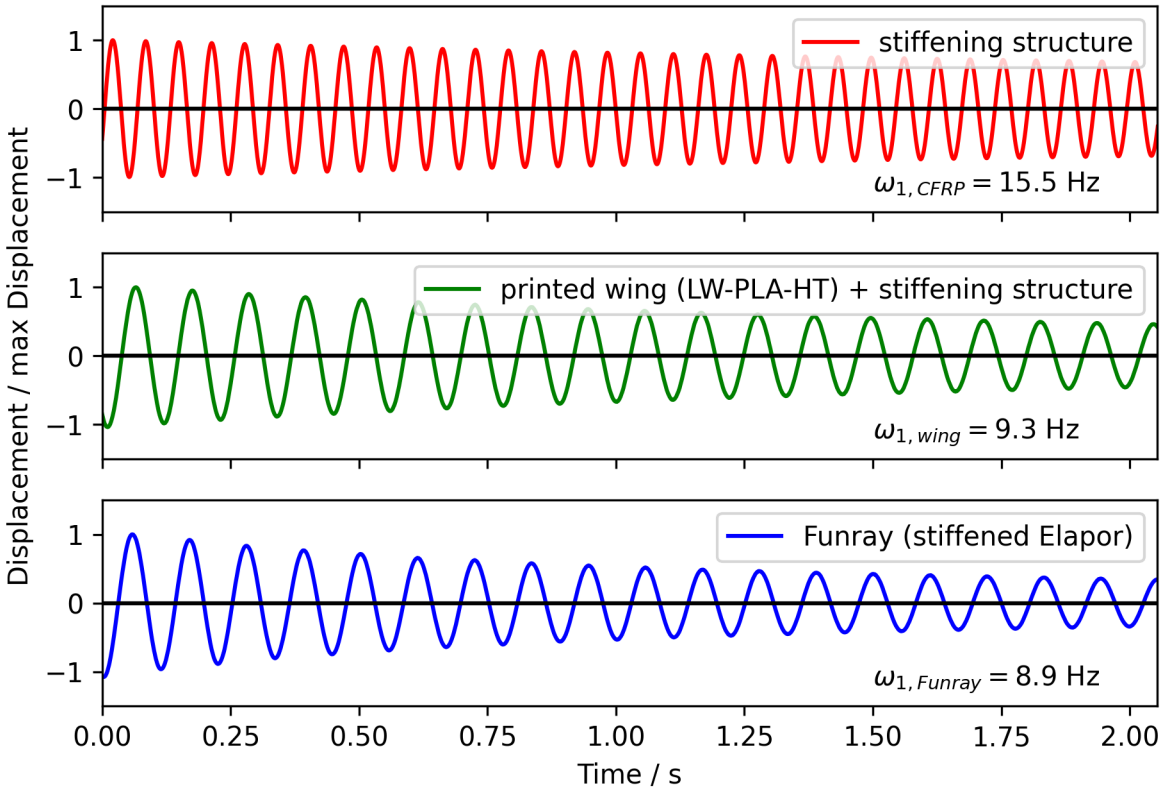


Figure 8 – Comparison of the normalized frequency response of the stiffening structure, the stiffened printed wing and and the Funray Wing (stiffened Elapor) after an initial deflection.

### 4.3 Dynamic Analysis

The dynamic analysis uses the same experimental setup as the static investigation. Only the cameras had to be switched in order to realize a higher frame rate of 2000 Hz, which is well above the expected vibration frequencies. This change in cameras reduces the recording area to the tip of the wing and about 200 mm of the outer wing section.
Typically, a continuous excitation by a shaker with a defined frequency or the impact of a modal hammer is used to excite the structure. In the performed test the deflection of the wing tip was chosen instead, due to the brittle printed surface and the known shape of the first mode shape. In addition to the already-present printed wing and its stiffening structure, the wing of a comparable commercial available RC plane, the Funray, was also tested. The oscillation measurement are shown in Fig. 8. The Fast Fourier Transform (FFT) method was used to identify the natural frequencies shown in Tab. 3.

Table 3 – First natural frequencies of the investigated wing structures.

| | Funray Wing | stiffened printed Wing | stiffening structure |
|---|---|---|---|
| $\omega_1$ | 8.9 Hz | 9.3 Hz | 15.5 Hz |

When comparing the stiffening structure and the stiffened printed wing, the stiffening structure has the highest natural frequency, that is reduced by the addition of the foamed LW-PLA structure. It also increases the decay constant, which shortens the time frame that a gust will affect. The first natural frequency of the Funray and printed wing are close, it is also visible that the dampening of the Funray oscillation is even higher, despite the difference in stiffness and weight.

## 5. Summary and Outlook

In this investigation the reference configuration SE$^2$A MR,V 4 BW was scaled using a demonstrative scaling scheme that matches the Froude number and the relative density of both the MS and FS. Additional regulatory constraints defined the above ground level to be less than 120 m and also limited the weight to 25 kg. Together with the corresponding atmospheric data this resulted in the presented scaling scheme. The geometric scaling of 5.6 % coupled with a weight of 25 kg lead to a design with a considerable wing load of 480 N/m², which is considerably high when compared to typical RC planes. Therefore, it needs to be checked whether the thin printed wing surface in combination with the internal supports is able to withstand these aerodynamic loads. The currently followed approach to mitigate this problem is to build the aircraft structure itself much lighter while dedicated weights are added later in order to match the scaling of the targeted first natural frequency.
In an experimental investigation of the outer wing section compared to the Funray wing, it was shown that the manufacturing of the stiffened 3D printed wing is possible and that the produced structure can withstand the applied bending loads induced by a discrete force applied to the wing tip representing the real distributed load. The measured natural frequency of 9.3 Hz is close to the Funray wing (8.9 Hz) and the first bending mode of the full scale MR V4 at 9.84 Hz. The high bending deformation and rather low frequency is a good result considering the required speed of the actuators used in the active gust load alleviation and is thus easing the first flight experiments. From a scaling point of view, the frequencies still have to be increased by a factor of 4 to reach the similarity requirements. Since a flexible wing is to be investigated and a certain deformation at the wing tip in the range of 20 to 30 mm at 1g cruise flight is required to show a visible effect of the gust load alleviation, the internal weight and mass distribution as well as the connection of the wing to the fuselage must be investigated further and modified accordingly.

## 6. Contact Author Email Address

al.herwig@tu-braunschweig.de

## 7. Acknowledgments

We would like to acknowledge the funding by the Deutsche Forschungsgemeinschaft (DFG, German Research Foundation) under Germany's Excellence Strategy **EXC 2163/1** - Sustainable and Energy Efficient Aviation - **Project ID 390881007**.

## 8. CRediT authorship contribution statement

**A. Herwig:** Conceptualization, Methodology, Software, Validation, Formal analysis, Investigation, Resources, Data Curation, Writing - Original Draft, Writing - Review & Editing, Visualization, Project administration **Matthias Haupt:** Conceptualization, Methodology, Resources, Funding acquisition.**Tristan Brack:** Methodology, Software, Validation, Writing - Review & Editing. **Jorge Bustamante:** Writing - review & editing. **Sebastian Heimbs:** Resources, Funding acquisition, Review & Editing.

## 9. Copyright Statement



## References

[1] European Commission, Directorate-General for Mobility and Transport, Directorate-General for Research and Innovation. *Flightpath 2050: Europe's vision for aviation: Maintaining global leadership and serving society's needs*. Luxembourg: Publications Office of the European Union, 2012. DOI: 10.2777/15458.

[2] Christian Wallace et al. "Evaluation environment for cascaded and partly decentralized multirate load alleviation controllers". In: *33rd congress of the international council of the aeronautical sciences, ICAS 2022* (Sept. 2022).

[3] Stanislav Karpuk, Rolf Radespiel, and Ali Elham. "Assessment of future airframe and propulsion technologies on sustainability of next-generation mid-range aircraft". In: *Aerospace* 9.5 (May 2022), p. 279. DOI: 10.3390/aerospace9050279.

[4] National Geophysical Data Center. "U.S. standard atmosphere (1976)". In: *Planetary and Space Science* 40.4 (Apr. 1992), pp. 553–554. DOI: 10.1016/0032-0633(92)90203-Z.

[5] André Bauknecht et al. "Novel concepts for active load alleviation". In: *AIAA SCITECH 2022 Forum*. San Diego, CA & Virtual: American Institute of Aeronautics and Astronautics, Jan. 2022. DOI: 10.2514/6.2022-0009.

[6] Yannic Beyer et al. "An aeroelastic flight dynamics model for gust load alleviation of energy-efficient passenger airplanes". In: *AIAA AVIATION 2023 Forum*. San Diego, CA and Online: American Institute of Aeronautics and Astronautics, June 2023. DOI: 10.2514/6.2023-4452.

[7] Jonathan. E. Cooper et al. "Design of a Morphing Wingtip". In: *Journal of Aircraft* 52.5 (Sept. 2015), pp. 1394–1403. DOI: 10.2514/1.C032861.

[8] Patrick Meyer, Hendrik Traub, and Christian Hühne. "Actuated adaptive wingtips on transport aircraft: Requirements and preliminary design using pressure-actuated cellular structures". In: *Aerospace Science and Technology* 128 (2022). DOI: 10.1016/j.ast.2022.107735.

[9] Daniel Hahn and Matthias Haupt. "Exploration of the effect of wing component post-buckling on bending-twist coupling for nonlinear wing twist". In: *CEAS Aeronautical Journal* 13.3 (July 2022), pp. 663–676. DOI: 10.1007/s13272-022-00586-2.

[10] Daniel Hahn, Matthias Haupt, and Sebastian Heimbs. "Passive Load Alleviation by Nonlinear Stiffness of Airfoil Structures". In: *AIAA SCITECH 2022 Forum*. San Diego, CA & Virtual: American Institute of Aeronautics and Astronautics, Jan. 2022. DOI: 10.2514/6.2022-0318.

[11] Alejandro Sobron, David Lundström, and Petter Krus. “A review of current research in subscale flight testing and analysis of its main practical challenges”. In: *Aerospace* 8.3 (2021), p. 74. DOI: 10.3390/aerospace8030074.

[12] Bruce Owens et al. “Overview of dynamic test techniques for flight dynamics research at NASA LaRC”. In: *25th AIAA aerodynamic measurement technology and ground testing conference*. 2006. DOI: 10.2514/6.2006-3146.

[13] Zhiqiang Wan and Carlos E. S. Cesnik. “Geometrically Nonlinear Aeroelastic Scaling for Very Flexible Aircraft”. In: *AIAA Journal* 52.10 (Oct. 2014), pp. 2251–2260. DOI: 10.2514/1.J052855.

[14] Thomas G. Gainer and Sherwood Hoffman. *Summary of transformation equations and equations of motion used in free flight and wind tunnel data reduction and analysis*. Tech. rep. 1972.

[15] Chester H. Wolowicz, James S. Bowman Jr., and William P. Gilbert. “Similitude requirements and scaling relationships as applied to model testing”. In: (1979).

[16] Alejandro Sobron. *On Subscale Flight Testing : Applications in Aircraft Conceptual Design*. en. Vol. 1819. Linköping Studies in Science and Technology Thesis. Linköping: Linköping University Electronic Press, Nov. 2018. DOI: 10.3384/lic.diva-152488.

[17] Edgar Buckingham. “On physically similar systems; illustrations of the use of dimensional equations”. In: *Physical Review* 4.4 (Oct. 1914), pp. 345–376. DOI: 10.1103/PhysRev.4.345.

[18] Multiplex. *Elektro-Segelflugmodelle - RR FUNRAY*. June 2024.

[19] colorFabb. *Technical datasheet - light-weight PLA - colorFabb LW-PLA-HT*. Nov. 2023.